Supplementary Information for "High-Resolution Faraday Rotation and Electron-Phonon Coupling in Surface States of the Bulk-Insulating Topological Insulator $Cu_{0.02}Bi_2Se_3$"

Liang Wu,[1,*] Wang-Kong Tse,[2,3] M. Brahlek,[4,†] C. M. Morris,[1] R. Valdés Aguilar,[1,5] N. Koirala,[4] S. Oh,[4] and N. P. Armitage[1,‡]

[1]*The Institute for Quantum Matter, Department of Physics and Astronomy, The Johns Hopkins University, Baltimore, Maryland 21218 USA.*
[2]*Theoretical Division, Los Alamos National Laboratory, Los Alamos, New Mexico 87545, USA.*
[3]*Department of Physics and Astronomy, MINT Center, University of Alabama, Tuscaloosa, Alabama 35487, USA*
[4]*Department of Physics and Astronomy, Rutgers the State University of New Jersey, Piscataway, New Jersey 08854 USA.*
[5]*Department of Physics, The Ohio State University, Columbus, Ohio 43210, USA.*

I. MATERIALS AND EXPERIMENTAL METHODS

Standard time-domain THz spectroscopy (TDTS) in a transmission geometry was performed with a custom home-built THz spectrometer. In this technique an approximately single-cycle picosecond pulse of light is transmitted through the sample and the substrate. The complex transmission is obtained from the ratio of a Fourier transformed time-domain sample pulse over a Fourier transformed substrate pulse. The complex conductance can be directly inverted from the transmission equation in the thin film limit[1,2]:

$$\tilde{T}(\omega) = \frac{1+n}{1+n+Z_0 G(\omega)} e^{i\omega(n-1)\Delta L/c} \tag{1}$$

where ΔL is the small difference in thickness between the sample and reference substrates, n is the real index of refraction of substrate and Z_0 is the vacuum impedance, 376.7 Ω. By measuring both the magnitude and phase of the transmission, this inversion to conductance is done directly and does not require Kramers-Kronig transformation. TDTS is an ideal tool to study the low frequency response of these materials with both the metallic Drude peak and a E_{1u} infrared active phonon visible.

Thin films of $Cu_{0.02}Bi_2Se_3$ were grown at Rutgers University by molecular beam epitaxy (MBE) on 0.5 mm thick crystalline Al_2O_3 substrates. Details on the growth can be found elsewhere[3,4]. Films grow a quintuple layer (1 unit cell) at a time (1 QL∼1 nm). After film growth, a 100 nm amorphous Se cap is deposited to reduce aging effects[5]. Se capping was shown to have a negligible contribution to the optics at THz frequencies[2], yet it serves a very important protection layer as Cu doped Bi_2Se_3 is much less stable in air than pure Bi_2Se_3. 3-4% optimal Cu concentration (Cu/Bi×100%) was incorporated during the film deposition and the concentration can be controlled at better than the 1% level. Therefore, the 'x' in $Cu_xBi_2Se_3$ formula is 0.015-0.02. Samples were sealed in vacuum and sent immediately to JHU and low temperature TDTS measurements began within 24 hours of their growth. The samples were mounted inside an optical helium flow cryostat and cooled down to 5 K within an hour.

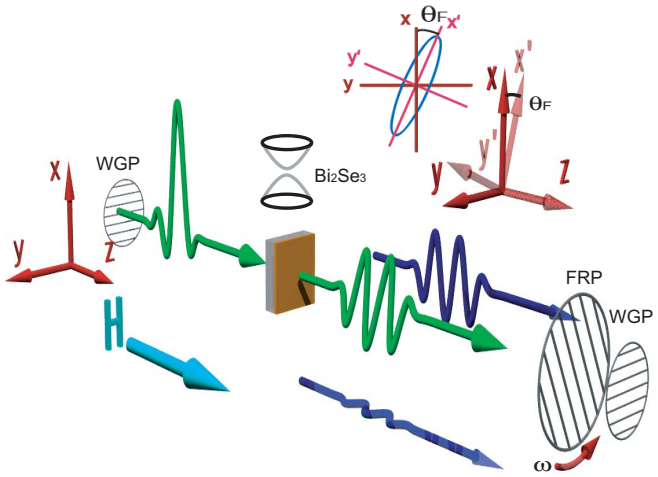

FIG. 1: (Color online) Demonstration of experimental setup for Faraday rotation experiments.

Complex Faraday rotation measurements were performed in a closed-cycle 7 T superconducting magnet at 5 K. We use the polarization modulation technique to measure the polarization states accurately[6]. As shown in Fig. 1, a static wire-grid polarizer (WGP1) is placed before the sample. After the sample, a fast rotating polarizer (FRP) unit and another static WGP2 are used. WGP1 and WGP2 transmit vertically polarized light. With this combination, in the polarization modulation technique, $E_x(t)$ and $E_y(t)$ (blue pulses) can be measured simultaneously in a single scan by reading off the in- and out-of-phase outputs from a lockin. Complex Faraday rotation $\theta_F = \theta_F^{'} + i\theta_F^{''}$ can be obtained by θ_F=atan$[E_y(\omega)/E_x(\omega)]$ after Fourier transforming into the frequency domain. Linearly polarized light becomes elliptically polarized after passing through the sample with a Faraday rotation $\theta_F^{'}$ (real part). The imaginary part of the Faraday rotation $\theta_F^{''}$ is related to the ellipticity in the small rotation angle regime[6]. In these measurements, a small background rotation from misalignment was subtracted by measuring a blank substrate.

II. MORE DATA AND ANALYSIS FOR $Cu_{0.02}Bi_2Se_3$ AND Bi_2Se_3

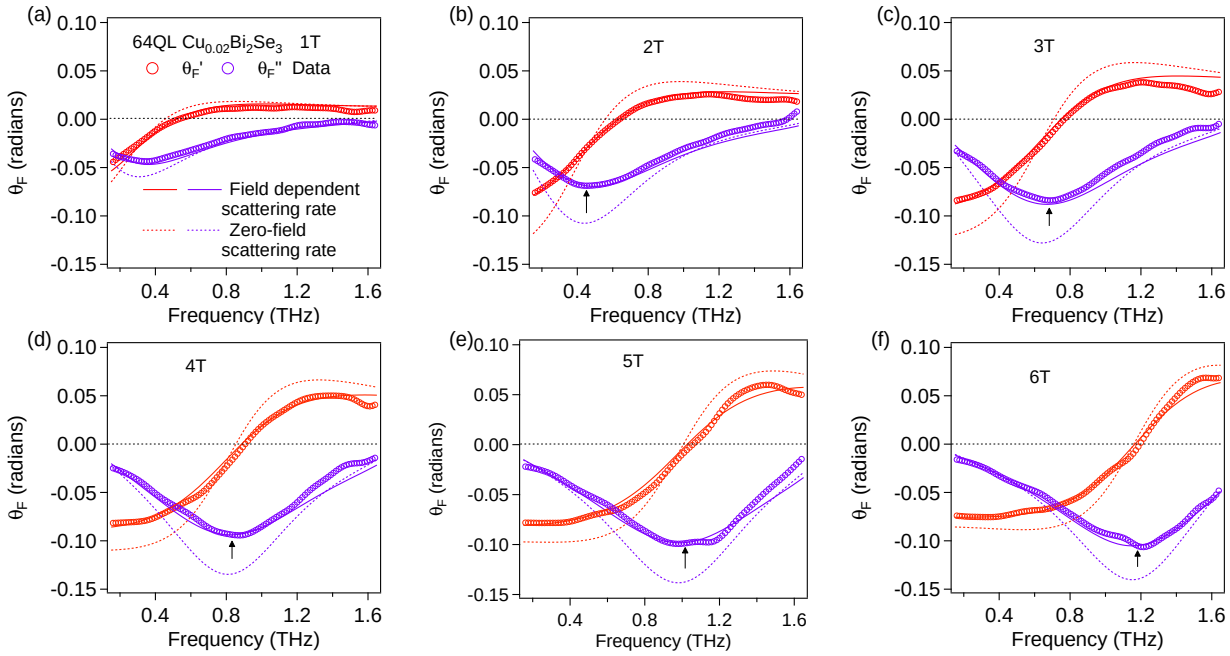

FIG. 2: (Color online) Fit quality on 64 QL $Cu_{0.02}Bi_2Se_3$ (sample 1) at different fields. Arrows are guides to the eye for the cyclotron frequencies. Accurate numbers were determined by fits. Solid lines are fits with field-dependent scattering rates. Dashed lines are fits using the zero-field scattering rates.

The carrier density of each TSS can be calculated by the usual relation $n_{2D} = k_F^2/4\pi$. An effective transport mass $m^* = \hbar k_F/v_F$ can still be defined for even for 'massless' Dirac fermions where the Fermi velocity is determined by $v_F = \partial E_F/\hbar\partial k$. In our analysis we will consider up to quadratic dispersion for surface states ($E = Ak_F + Bk_F^2$) and model the two surface states as identical with same carrier density. Considering the TSS dispersion up to quadratic correction, the spectral weight can be expressed in terms of k_F[7].

$$\frac{2}{\pi\epsilon_0}\int G_{D1}d\omega = \omega_{pD}^2 d = \frac{k_F(A+2Bk_F)e^2}{2\pi\hbar^2\epsilon_0} \tag{2}$$

Therefore, lower spectral weight means lower k_F. Lower k_F means lower carrier density and smaller mass. By fitting the zero-field conductance, we find $(\omega_{pD}/2\pi)^2 d$ in the 64 QL $Cu_{0.02}Bi_2Se_3$ sample 1 (the one discussed in main text) equal to 3.0±0.2 × 10^4 THz^2 · nm. By using Eq. 2, we obtain k_F= 0.056±0.003 Å^{-1}, E_F = 145 ±5 meV, m^* =0.135±0.005 m_e and a total sheet carrier density n_{2D}=5.0 ±0.3 ×10^{12}/cm^2. From the Faraday rotation fit, we get the spectral weight $(\omega_{pD}/2\pi)^2 d$ = 2.8 ± 0.1 × 10^4 THz^2· nm more accurately. By using the relation $\omega_{pD}^2 d = \frac{n_{2D}e^2}{m^*\epsilon_0}$ and effective mass from CR experiments, we can get carrier density n_{2D} = 4.9 ± 0.1 × 10^{12}/cm^2. These two analysis agree self-consistently. Here we have shown a new way to self-consistently study surface state transport.

Here we show all the data and fits for both 64 QL $Cu_{0.02}Bi_2Se_3$ samples (sample 1 and sample 2) . One can see in Fig. 2 for $Cu_{0.02}Bi_2Se_3$ (sample 1) that the difference in fits between field independent and field dependent scattering rates are highly distinguishable at finite fields, which is another indication of increasing scattering rate due to electron-phonon coupling.

We observed similar phenomena on another 64 QL $Cu_{0.02}Bi_2Se_3$ (sample 2) and reached a similar conclusion to sample 1. This sample 2 remained bulk-insulating and with high-mobility after 8 months of exposure to air, which demonstrates the realization of a robust bulk-insulating TI by the protection of Se capping. This sample also had $\sim 5.0 \times 10^{12}/\mathrm{cm}^2$ but slightly lower mobility $\sim 2800\ \mathrm{cm}^2/\mathrm{V{\cdot}s}$. Data and fitting results are shown in Fig. 3. Here we subtracted the zero-field 'rotation' as a small background from misalignment, which gives the same result as a substrate background is subtracted. We also performed extended Drude analysis and reached a similar conclusion to sample 1. Suppression of the scattering rate at low frequency was observed and a coupling constant in the DC limit $\lambda \sim 0.50 \pm 0.05$ is extracted. As discussed in the main text, electron-phonon coupling is not sensitive to magnetic field itself. This is what we showed by showing the extended Drude model analysis at zero magnetic field gives a overall similar frequency dependence. The magnetic field rather, changes how electron phonon coupling manifests itself in the spectra. One generally expects that such coupling causes broadening of some spectral feature at frequencies overlapping with a characteristic phonon energy. By putting on a magnetic field one pushes the zero frequency Drude peak to higher frequency and causes it to broaden. The electron-phonon coupling can be seen either by pushing the Drude peak across the characteristic phonon frequencies with magnetic field or by looking at subtle deviations from a Lorentzian lineshape at frequencies above the phonon frequencies in zero field. Basically, we can view the magnetic field as a energy sampling tool.

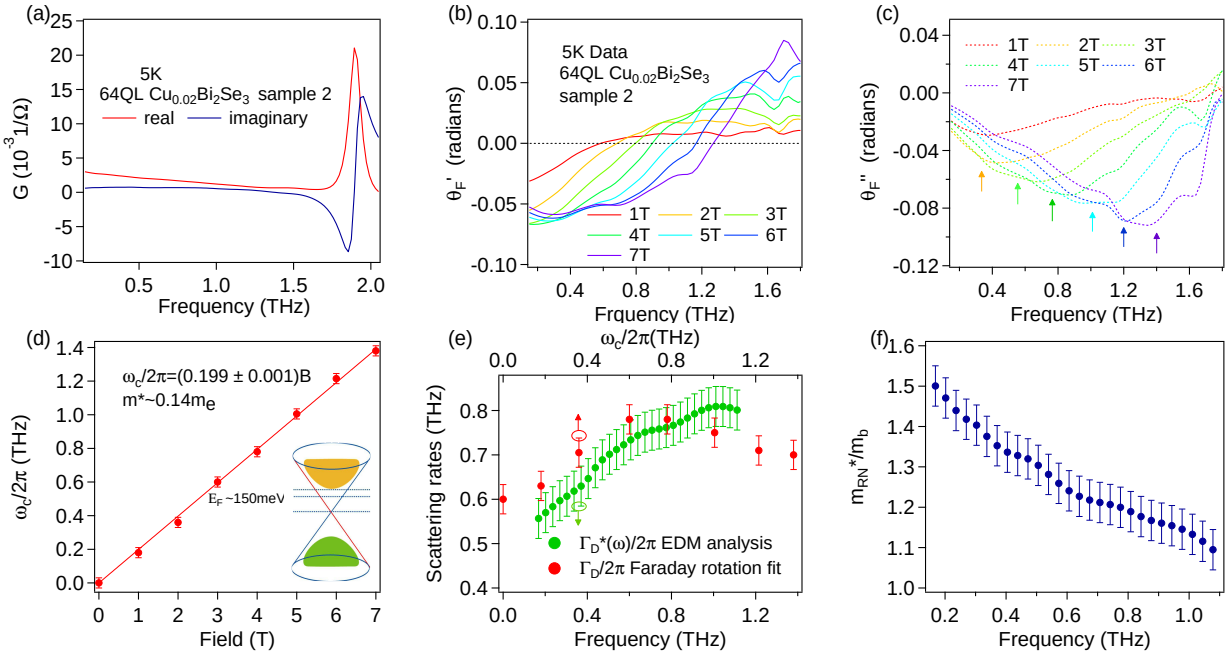

FIG. 3: (Color online) Data summary on 64 QL $Cu_{0.02}Bi_2Se_3$ (sample 2) which was exposed in air for 8 months. (a) Complex conductance at 5 K. (b) Real and (c) Imaginary part of complex Faraday rotation data at different fields at 5 K. (d) Cyclotron frequency versus field. The inset is a cartoon indicating E_F ~150 meV, 70 meV below conduction band minimum. (e) Scattering rate as a function of cyclotron frequency (red). Renomalized scattering rate by mass through extended Drude analysis (green) as a function of frequency. (f) Renormalized mass as a function of frequency. The error bars express the uncertainty in ω_{pD} .

In Fig. 4, we show the fits for 100 QL Bi_2Se_3. This demonstrates that a single channel is the principal contribution to the CR and dominates the Faraday rotation. This channel has spectral weight $(\omega_p/2\pi)^2 d = 7.6 \pm 0.3 \times 10^4\ \mathrm{THz}^2 \cdot \mathrm{nm}$. We use the spectral weight ($\omega_p^2 d = \frac{n_{2D}e^2}{m^*\epsilon_0}$) and CR mass 0.20 m_e to extract a total sheet carrier density $n_{2D} \sim 1.9 \pm 0.1 \times 10^{13}/\mathrm{cm}^2$. If using Eq. 2 with the TSS dispersion, from spectral weight we find $k_F \sim 0.11\ \mathrm{Å}^{-1}$, $n_{2D} \sim 2.0 \times 10^{13}/\mathrm{cm}^2$, m^* ~0.20 m_e and $E_F \sim 350$ meV, which agrees with ARPES results on the similar samples[8]. Agreement between these two analyses self-consistently assign this channel to topological surface states. Considering that the characteristic penetration depth of the TSS is of order 2 nm[2,9], ≈7 ° rotation per surface is an extremely large rotation per unit length. The second channel gives a small flat background. In the CR fits of 100 QL Bi_2Se_3, we fixed the scattering rate of the low mobility channel to 4 THz as we obtained from zero-field conductance fits, but the fits are reasonably insensitive to the precise scattering rate of this channel. Field dependent scattering of the TSS channel of the 100 QL Bi_2Se_3 is shown in Fig. 5 and the same basic physics as $Cu_{0.02}Bi_2Se_3$ was found. Considering twice more free parameters in the fits resulted from multiple channel conduction, we are not able to extract field dependent scattering of the TSS channel of the 100 QL Bi_2Se_3 as reliable as the $Cu_{0.02}Bi_2Se_3$ case. Also because of two Drude coexistence,

extended Drude analysis is not reliable to extract coupling strength even though suppression of scattering rate at low frequency is also observed. Another reason is that it is likely that substantial charge impurity scattering comes from Se defects at the back interface and compete with electron-phonon scattering as the former usually give a decreasing scattering rate with magnetic field[10]. However, electron-phonon coupling is normally expected not to be sensitive to doping and we believe a similar electron-phonon coupling exists in undoped Bi_2Se_3. It is just that the development of truly insulating $Cu_{0.02}Bi_2Se_3$ system gives a simpler spectra that allows us to determine the field dependent scattering rate systematically and provide quantitative measures of the electron-phonon coupling.

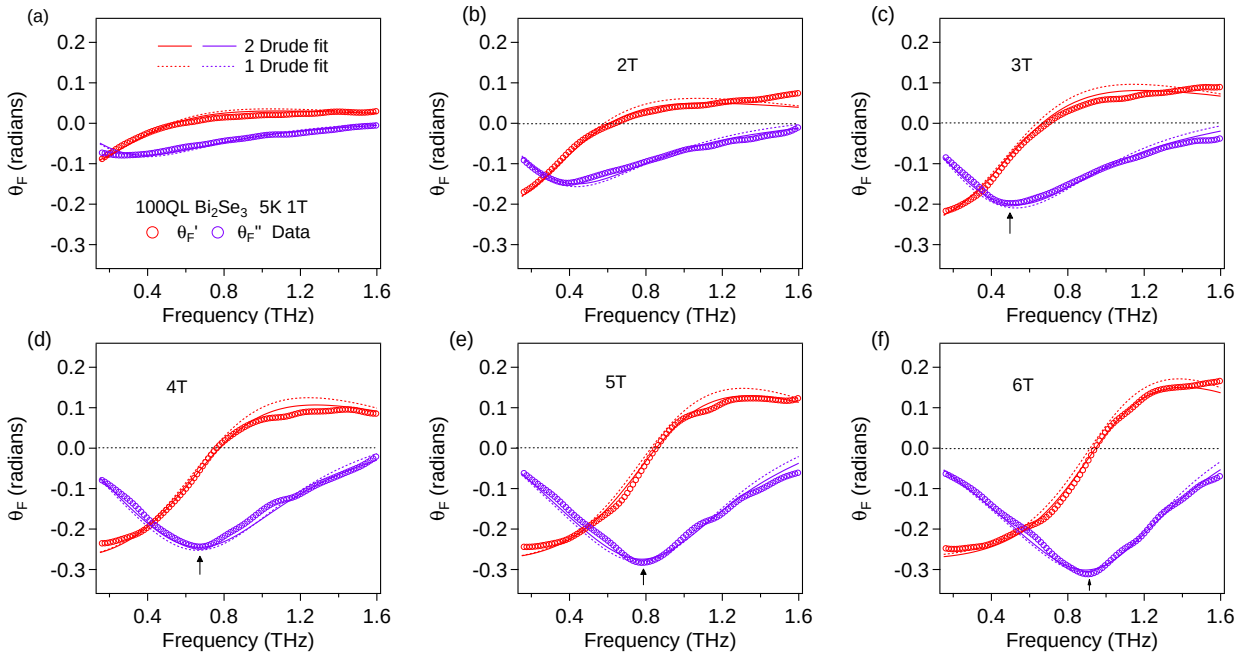

FIG. 4: (Color online) Fit quality on 100 QL Bi_2Se_3 at different fields. The solid curves are fits using two Drude terms. Dashed curves are with one Drude term. Arrows are eye guides for cyclotron frequencies. Accurate numbers were determined by fits.

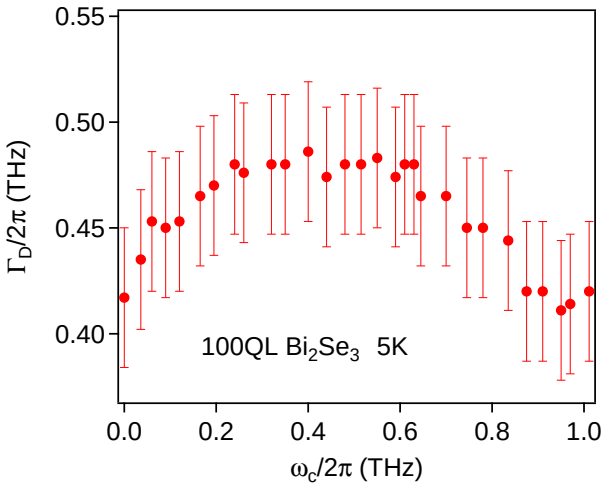

FIG. 5: (Color online) Drude scattering rate of 100 QL Bi_2Se_3 as a function of cyclotron frequency at 5 K.

A 32 QL Bi_2Se_3 was also measured. Data summary is shown as Fig. 6. The channel that dominates CR has an effective mass m^* ~0.19m_e, carrier density n_{2D} ~ 1.90×10^{13}/cm^2 and mobility μ ~2000 cm^2/V·s, which is consistent with TSSs with E_F ~ 310 meV above the Dirac point. A second channel with scattering rate ~ 4 THz is added to fit zero-field conductance. By using the effective mass of bulk/2DEG from literature, the second channel has total sheet carrier density ~ 0.8×10^{13}/cm^2 and mobility

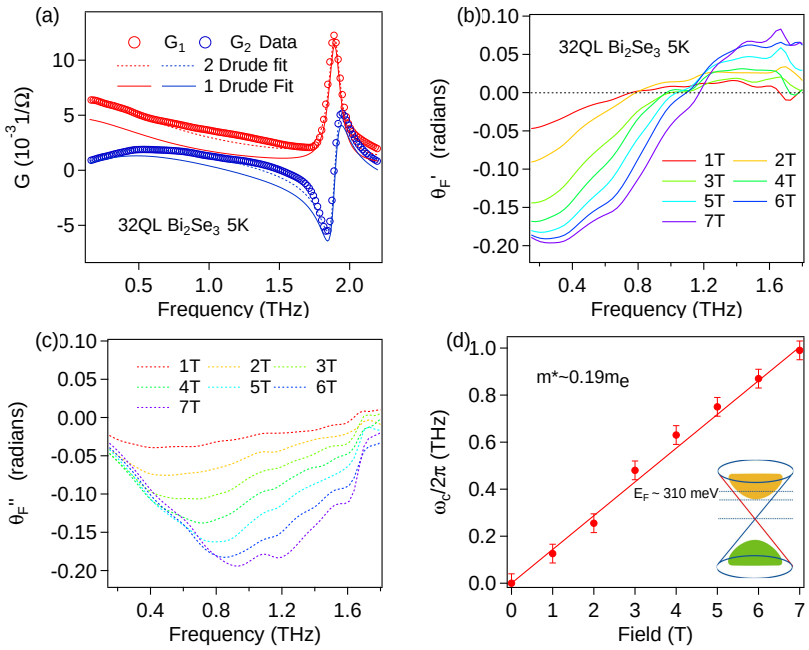

FIG. 6: (Color online) Data summary on 32 QL Bi_2Se_3 at 5 K. (a) Complex conductance at 5 K. Solid lines are 1 Drude fits using parameters obtained from fitting the Faradary rotation with 1 Drude term. Dashed lines are 2 Drude fit. (b)Real and (c) Imaginary Faraday rotation at different fields. (d) Cyclotron frequencies as a function of field. Solid line is a linear fit of $\omega_c = eB/m^*$. The inset is a cartoon indicating E_F ~310 meV.

less than 300 $cm^2/V\cdot s$.

Note that the Faraday rotation spectra for Bi_2Se_3 and $Cu_{0.02}Bi_2Se_3$ looks similar in shape at first glance, but they are different in two ways. Firstly and obviously, CR frequencies is different, which gives a different mass. Secondly and most importantly, they indicate two samples are in completely different regime in terms of observation of quantized Faraday/Kerr rotation. Ref.[11] proposed 90 degree Kerr rotation and Faraday rotation with value of fine structure $\alpha \sim 7.3$ mrad when chemical potential is in the lowest Landau Level (LL) in free standing films. Kerr rotation and Faraday rotation give the same information because ultimately it traces back to half-integer quantum hall effect in the conductance. In free standing films in the quantum regime, Faraday rotation is $tan(\theta_F) = \alpha(\nu_t+1/2+\nu_b+1/2)$, where ν_t and ν_b are LL filling factors for top and bottom surface states. In real experiments, free standing films are difficult to reach. People usually measure films on substrate and therefore renormalization from substrate effects come in. In the quantum hall regime, $tan(\theta_K) = \frac{4n\alpha}{n^2-1}(\nu_t + 1/2 + \nu_b + 1/2)\sim$ 10 mrad $\times(\nu_t + 1/2 + \nu_b + 1/2)$, $tan(\theta_F) = \frac{2\alpha}{1+n}(\nu_t + 1/2 + \nu_b + 1/2)\sim$3.5 mrad $\times(\nu_t + 1/2 + \nu_b + 1/2)$. In this regards, Ref.[1] with 65 degree Kerr rotation has never reached the quantum hall regime because chemical potential is way in the conduction band, which is not a topological insulator at all. From Bi_2Se_3 to $Cu_{0.02}Bi_2Se_3$, we pushed LL filling factor $\nu \sim 40$ to $\nu \leq 10$ with 7 Tesla magnet. The Laudau Level energy spectrum is $E(\pm\nu) = \pm v_F\sqrt{2e\hbar B \mid \nu \mid}$, where $\pm$ stands for electron and holes representatively. With experimentally achievable magnet field such as pulse magnet facility at Los Alamos National Laboratory, 150 T is enough to push the chemical potential into lowest LL and observe the quantized Faraday rotation. We just need to wait the THz system with pulse field finish its construction. Recall that scattering rate in $Cu_{0.02}Bi_2Se_3$ is only less than 2 meV, so LLs will be well separated in energy. The threshold for magnetic field to reach lowest LL can be reduced further by combining with gating. Also, we reduced resolution from 5 degree in Ref.[1] to 0.3 degree (0.5 mrad) in the current work. As discussed in the main text, our high-resolution Faraday rotation spectroscopy on $Cu_{0.02}Bi_2Se_3$ opens the new era to observed quantized Faraday rotation and topological magneto-electric effect, which are smoking guns for Dirac surface states.

III. TRANSPORT LIFETIME OF TOPOLOGICAL INSULATORS IN AN EXTERNAL MAGNETIC FIELD

In this section we investigate various possibilities for the increase in scattering rate at high magnetic fields deriving from effects due to the field itself.

A. Zeeman (Spin) Effect On Transport Lifetime Of Topological Insulators In An External Magnetic Field

In principle the canting of spins in the surfaces states due to Zeeman coupling under applied magnetic field can cause an increase in the scattering rate because back scattering can occur. In practice this is a very small effect at the current chemical potential levels. One can see this as follows.

In the topological regime where the bulk is insulating, one can describe the light-matter interaction of a topological insulator by the Hamiltonian of its surface states:

$$H_{\boldsymbol{k}} = v\boldsymbol{\sigma}\cdot(\boldsymbol{k}\times\hat{\boldsymbol{z}}), \tag{3}$$

where $\boldsymbol{k}$ is the electron momentum, v is the Fermi velocity, and $\boldsymbol{\sigma}$ is the Pauli matrix corresponding to the spin degrees of freedom. In an external out-of-plane magnetic field $\boldsymbol{B} = \nabla\times\boldsymbol{A}$ (where $\boldsymbol{A}$ the corresponding vector potential), the Hamiltonian Eq. (3) couples to the magnetic field through the orbital degrees of freedom with $\boldsymbol{k}\to\boldsymbol{k}-e\boldsymbol{A}/c$, and the spin degrees of freedom with $H_{\boldsymbol{k}}\to H_{\boldsymbol{k}}+\Delta$ where the Zeeman coupling $\Delta = -g_s\mu_B B/2$ acts like a Dirac mass term. We examine the effect due to each coupling on the transport lifetime.

In low magnetic fields, the effect of magnetic field on the transport lifetime is largely due to the spin polarization effect from Zeeman coupling. Therefore we first consider the regime $\omega_c\tau_{tr}, |\Delta|\tau_{tr}\ll 1$, where $\omega_c = eBv/\hbar k_F$ is the cyclotron frequency. It will be convenient to derive the Zeeman field dependence of the transport lifetime τ_{tr} using the quantum kinetic theory[12]. The kinetic equation for the momentum-dependent charge-spin density matrix f_k is

$$\frac{\partial f_k}{\partial t} + i[H_k+\Delta\sigma_z, f_k] + \frac{1}{2}\left[e\boldsymbol{E}+\frac{e}{c}\boldsymbol{v}_k\times\boldsymbol{B}, \frac{\partial f_k}{\partial\boldsymbol{k}}\right]_+ = J(f_k|\boldsymbol{k},t), \tag{4}$$

where $\boldsymbol{E}$ is the external A.C. electric field from the incident light, $\boldsymbol{v}_k = \partial H_k/\partial\boldsymbol{k} = v(\hat{\boldsymbol{z}}\times\boldsymbol{\sigma})$ is the single-electron velocity operator, and $[\ ,\ ]_+$ is the anti-commutator. $J(f_k|\boldsymbol{k},t)$ denotes the collision integral containing information about scattering rates. Note that Zeeman coupling mixes different spins and gives rise to a "spin canting" effect, opening up a spin-flipping channel through electron-impurity scattering. A related problem was studied in the literature in the context of the anomalous Hall effect of topological insulators due to magnetic impurities[13].

We first start by decomposing the density matrix as $f_k = f_k^{(0)} + \delta f_k$, where $f_k^{(0)}$ is the equilibrium distribution function and δf_k is the non-equilibrium part. We can facilitate the solution of Eq. (4) by resolving δf_k into components of projected onto the charge and spin sectors: $\delta f_k = n_k + \boldsymbol{s}_k\cdot\boldsymbol{\sigma}$, where n_k and $\boldsymbol{s}_k$ describe the charge and spin density distributions respectively. For the semiclassical weak-field regime we are studying in this section, the Drude response is given by the conductivity to leading order in $1/E_F\tau_{tr}$, and the transport lifetime is determined only by the dynamics of n_k and the component of $\boldsymbol{s}_k$ projected along the electron's spin direction at the momentum $\boldsymbol{k}$. We find the momentum relaxation rate as

$$\frac{1}{2\tau_k} = \frac{n_i\varepsilon_k}{4v^2}\int_0^{2\pi}\frac{\mathrm{d}\phi_{k'k}}{2\pi}|u(k,\phi_{k'k})|^2\,(1-\cos\phi_{k'k})\left(1+\cos^2\theta_k+\sin^2\theta_k\cos\phi_{k'k}\right), \tag{5}$$

where $\phi_{k'k}$ is the angle between the momenta $\boldsymbol{k}$ and $\boldsymbol{k}'$, $\sin\theta_k = vk/\varepsilon_k$ and $\cos\theta_k = \Delta/\varepsilon_k$ with $\varepsilon_k = \sqrt{(vk)^2+\Delta^2}$, n_i is the impurity concentration, and $|u(k,\phi_{k'k})|^2$ is the disorder-averaged impurity potential evaluated at momentum $k' = k$. In the absence of a magnetic field such that $\Delta = 0$, the angular form factors in Eq. (5) reduce to the standard expression $(1-\cos^2\phi_{k'k})$ which describes the suppression of back scattering of TSS.

We can further model the impurity potential as short-range delta-function scatters with $|u(k,\phi_{k'k})|^2\equiv u_0^2$ being independent of k. The transport lifetime is determined by Eq. (5) at the Fermi level at low temperatures $k_BT\ll E_F$. Evaluating the angular integral, we then obtain the transport lifetime in the weak magnetic field regime

$$\frac{1}{2\tau_{tr}} = \frac{n_i u_0^2 E_F}{8v^2}\left[1+3\left(\frac{g_s\mu_B B}{2E_F}\right)^2\right]. \tag{6}$$

Denoting the zero-field transport scattering rate as $1/2\tau_{tr,0} = n_i u_0^2 E_F/8v^2$, the weak-field transport scattering rate $1/2\tau_{tr,B}$ is related to that in zero field as

$$\frac{1}{\tau_{tr,B}} = \frac{1}{\tau_{tr,0}}\left[1+3\left(\frac{g_s\mu_B B}{2E_F}\right)^2\right]. \tag{7}$$

If we use $g_s\sim 50$, $E_F\sim 150$meV, the spin effect only gives a 0.27% increase at 3 T, which is orders of magnitudes off from experiments. Therefore, we do not believe the Zeeman effect is the cause for the increase of scattering rate.

B. Orbital Effect On Transport Lifetime Of Topological Insulators In An External Magnetic Field

In this section, we consider the effect of orbital coupling to the magnetic field on the transport lifetime. The influence of impurity scattering on the density of states and magneto-transport properties of the electron system can be captured using the self-consistent Born approximation (SCBA)[14]. This approximation captures certain features of Landau level (LL) broadening due to disorder and is often sufficient to describe magnetotransport properties when localization effects are not important, as expected in optical experiments.

The SCBA for the case of graphene was discussed extensively in Ref. [15]. For our Cu-doped sample, we estimate from Faraday rotation and SdH oscillations[4] that the minimum occupied LL which occurs at the largest field $B = 7$ T is $n \sim 10$. Therefore, the Fermi level is far from the $n = 0$ Landau level (LL), and the effect of inter-LL coupling between opposite levels n and $-n$ is negligible. The LL spacing at the Fermi level is of the order of meV, which coincides with the energy scale of the scattering rate we extracted from our data [see Fig. 3(a) in main text]. This seems to suggest the sample would be in the regime where $\omega_c\tau_q \lesssim 1$, where $1/\tau_q$ is the single-particle lifetime that captures the LL disorder broadening (to be distinguished from $1/\tau_{tr}$ which is the transport lifetime we want to calculate. Generally $1/\tau_q > 1/\tau_{tr}$.)

The self-energy matrix is diagonal in the LL index and given by

$$\Sigma = \omega_c^2\rho\sum_{n=0}^{N_c}\frac{\varepsilon-\Sigma}{(\varepsilon-\Sigma)^2-\varepsilon_n^2}, \tag{8}$$

where we have defined the dimensionless parameter $\rho = n_i u_0^2/(4\pi v^2)$ that characterizes the disorder strength. Eq. (8) defines the self-consistency condition from which the self-energy can be solved. For high LL filling $|N| \gg 1$, one can use the approximation of extending the lower limit of the sum to $-N_c$ and setting $N_c \to \infty$, because the main contribution comes from the Fermi level and contributions from negative LLs and from N to ∞ amount to negligible errors.

Performing the sum in Eq. (8) using the Poisson summation formula,

$$\Sigma = \pi\rho\,(\varepsilon-\Sigma)\cot\left\{\frac{\pi}{\omega_c^2}\left[(\varepsilon-\Sigma)^2-\Delta^2\right]\right\}, \tag{9}$$

and then expanding the cot function into a Fourier series, we obtain

$$\Sigma'+i\Sigma'' = -i\pi\rho\,(\varepsilon-\Sigma'-i\Sigma'')\left\{1+2\sum_{k=1}^{\infty}\lambda_D^k\exp\left\{i\frac{2\pi k}{\omega_c^2}\left[(\varepsilon-\Sigma')^2-\Delta^2-(\Sigma'')^2\right]\right\}\right\}, \tag{10}$$

where we have denoted the real and imaginary parts of the self-energy as $\Sigma = \Sigma' + i\Sigma''$. λ is the so-called Dingle factor

$$\lambda_D = \exp\left\{-\frac{4\pi}{\omega_c^2}|\Sigma''|\,(\varepsilon-\Sigma')\right\}. \tag{11}$$

Eq. (10) is a nonlinear equation that needs to be solved iteratively. λ_D serves as the small parameter with which Eq. (10) can be solved for Σ up to first order in disorder correlation $\sim n_i u_0^2$ ($O(\rho^1)$) and to first order in λ_D ($O(\lambda_D^1)$).

First, in the zeroth order $O(\lambda_D^0)$ we have $\Sigma' = 0$ and $\Sigma'' = -(n_i u_0^2/4v^2)\varepsilon$. The latter can be identified as the quasiparticle scattering rate $1/2\tau_{q,0} = (n_i u_0^2/4v^2)\varepsilon$ at zero magnetic field.

To first order $O(\lambda_D^1)$, we obtain

$$\begin{aligned}\Sigma' &= \frac{1}{\tau_{q,0}}\varepsilon\lambda_D\sin\left[2\pi\left(\frac{\varepsilon^2-\Delta^2}{\omega_c^2}\right)\right],\\ \Sigma'' &= -\frac{1}{2\tau_{q,0}}\left\{1+2\lambda_D\cos\left[2\pi\left(\frac{\varepsilon^2-\Delta^2}{\omega_c^2}\right)\right]\right\}.\end{aligned} \tag{12}$$

The density of states is given by $\nu(\varepsilon) = 2\mathrm{Im}\Sigma/\omega^2\rho$, therefore we obtain from Eq. (12)

$$\nu(\varepsilon) = \nu_0(\varepsilon)\left\{1+2\lambda_D\cos\left[2\pi\left(\frac{\varepsilon^2-\Delta^2}{\omega_c^2}\right)\right]\right\}, \tag{13}$$

with $\nu_0(\varepsilon) = \varepsilon/2\pi v^2$ being the density of states at zero magnetic field.

Since the ratio of the transport scattering rate at finite field to that at zero field is equal to that of the density of states[16], finally we obtain

$$\frac{1}{\tau_{tr,B}} = \frac{1}{\tau_{tr,0}}\left\{1+2\lambda_D\cos\left[2\pi\left(\frac{E_F^2-(g_s\mu_B B/2)^2}{\omega_c^2}\right)\right]\right\}, \tag{14}$$

where $1/\tau_{tr,0} = n_i u_0^2 E_F/4v^2$ is the transport time at zero field.

In this scenario, the scattering rate should show magneto-oscillations above 3 T when $\omega_c \tau_{tr,B} \geq 1$. As we saw no such oscillations and only an increase in the scattering rate with field, we also rule out this possibility.

IV. EFFECT OF Se CAPPING

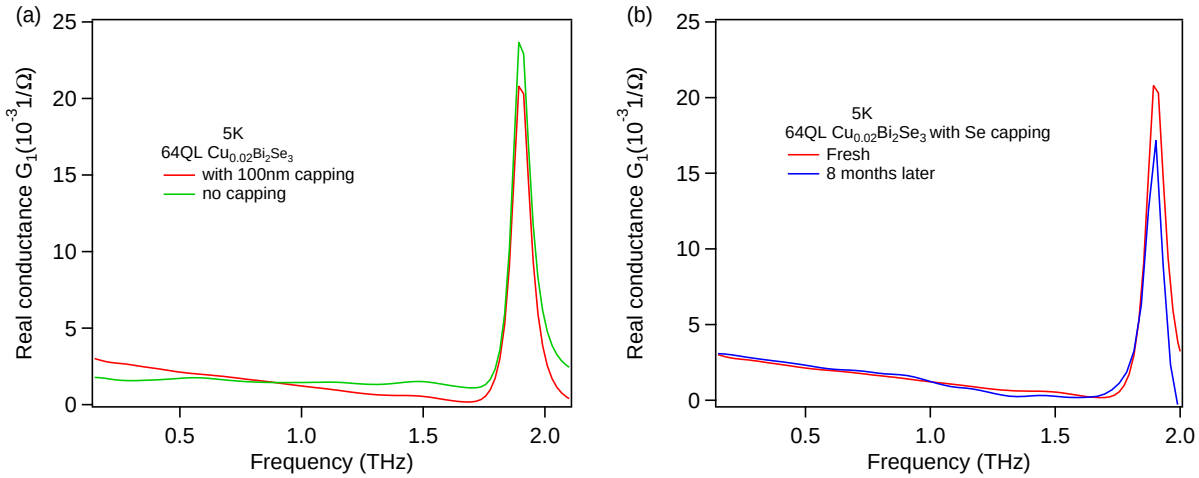

FIG. 7: (Color online) (a) Real conductance of 64 QL $Cu_{0.02}Bi_2Se_3$ (sample 2) with and without 100nm Se capping at 5 K . (b) Real conductance of 64 QL $Cu_{0.02}Bi_2Se_3$ (sample 2) with 100nm Se capping measured right after receiving the sample and 8 months later.

Our previous work on pure Bi_2Se_3 showed that Se capping had a negligible effect on the optical properties of Bi_2Se_3, but does decrease the scattering rate somewhat[2]. However, it is of great importance in the present case of Cu doped Bi_2Se_3 as these samples are very air sensitive. Transport measurements in Ref.[4] were performed right after samples were taken out of ultra-high vacuum MBE chamber. Samples for THz measurements were sealed in vacuum bags and shipped overnight to JHU. The total exposure to atmosphere is around 30 mins before loading into the cryostat and plus the overnight in the raw-vacuum bag. As one can see in Fig. 7(a), Se capping protects the mobility of the sample well as opposed to non-capped samples with a flat Drude component. 100nm Se capping still protects the sample well even after 8 months explosure in air as shown in Fig.7(b) on sample 2.

V. LIMITATIONS OF USING ONE DRUDE COMPONENT FIT IN PREVIOUS WORK[1,2]

For the 100 QL Bi_2Se_3 sample, if we fit the zero field conductance data by only a single Drude term, a phonon term and a ϵ_∞ term, we find the Drude spectral weight $(\omega_{pD}/2\pi)^2 d$ is 1.25×10^5 THz^2 · nm. Using Eq. 2, one gets k_F ~0.14 Å^{-1}, m^* ~0.22 m_e and E_F ~480 meV. We believe these values are overestimated and the low frequency spectral weight is actually comprised of two terms. As detailed above, a fit to the Faraday rotation data by one Drude term alone shows that the spectral weight $(\omega_{pD}/2\pi)^2 d$ contributing to the TSSs is only 7.6×10^4 THz^2 ·nm. Using Eq. 2, k_F ~0.11 Å^{-1}, m^* ~0.20 m_e and E_F ~ 350 meV are obtained, as already mentioned above. One can see E_F and k_F are overestimated by ~ 30%, while m^* is overestimated by ~ 10% if one associates all the Drude spectral weight in the zero-field conductance to the TSSs. These quantities are overestimated in the single Drude component model as one assigns all the bulk/2DEG spectral weight as the TSSs spectral weight. The second Drude channel (bulk/2DEG) is flat in our measurement frequency regime and only contributes a smooth background. However, considering the fact that the TSSs contribute more than 90% to the total conductance at low frequencies, a single Drude model analysis is still a good approximation and a thickness independent Drude peak as observed previously in Bi_2Se_3[1,2] is not surprising. The presence of this very flat subdominant contribution does not call into question any of the conclusions of our previous works[1,2]. Here we just clarify this point and provide a method to separate contributions from TSSs and bulk/2DEG in magneto-THz measurements.

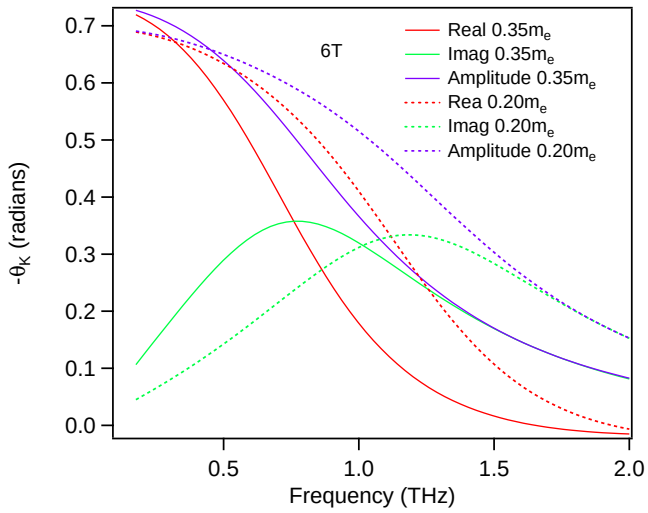

FIG. 8: (Color online) Calculation of various measures of the complex Kerr rotation with effective mass 0.35 m_e and mass 0.20 m_e with carrier density $n_{2D} = 2 \times 10^{13}/\text{cm}^2$ and scattering rate Γ_D=1 THz at 6 T.

VI. EFFECTIVE MASS INCONSISTENCY WITH PREVIOUS WORK[1]

In our earlier work[1], based on a fit with just a single Drude term, a heavier 0.35 m_e cyclotron mass for TSSs was reported. This was judged to be a reasonable number based on a linear dispersion of the TSSs as it gave a reasonable E_F ~0.5 eV using $m^* = E_F/v_F^2$ and $v_F = 5 \times 10^5$ m/s. However, there are a number of inconsistencies that this mass presents. If one considers quadratic corrections to the TSS dispersion, one finds that this mass does not give a consistent k_F. Moreover, if one uses a linear dispersion $E_F = \hbar v_F k_F$ and uses the spectral weight of a single Drude component to estimate the chemical potential, the relation is:

$$\omega_{pD}^2 d = \frac{\hbar v_F k_F e^2}{2\pi\epsilon_0\hbar^2} = \frac{E_F e^2}{2\pi\epsilon_0\hbar^2} \tag{15}$$

Here we assume two almost identical surface states. An analysis of the spectral weight gives E_F ~0.75 eV, which is unreasonably high. Therefore, when E_F is in the conduction band, quadratic corrections must be significant. One may note that in order that the wave functions of the TSSs vanish at the TI/vacuum interface, a quadratic correction is required[17,18]. In contrast, when we use Eq. 15 based on linear dispersion to estimate the chemical potential of $Cu_{0.02}Bi_2Se_3$, E_F is found to be 170 meV ± 10 meV. This better agreement is expected because surface state dispersions deviate from linearity less when E_F is closer to Dirac point. In summary, we believe that the CR mass 0.35 m$_e$ given in previous work Ref.[1] was incorrect for pure Bi_2Se_3 films and the revised value of 0.19-0.20 m_e given in this work is correct.

The reasons for this correction is multifold. 1.) Signal to noise has been improved by orders of magnitude in the current generation of experiments with polarization modulation technique with 0.5 mead resolution[6] allowing more reliable fits to the spectra. 2.) The current generation of Bi_2Se_3 films have mobilities of the order 2000 - 3200 cm^2/V· s^3. In order to see a well-defined cyclotron resonance in the dissipative response, the relation $\omega_c\tau = \mu B \geqslant 1$ needs to be satisfied. $\omega_c\tau = \mu B \sim$ 1.5-2 is still too small to see very sharp peaks in the amplitude of Kerr/Faraday rotation in our field range. 3.) In the previous work, due to (now overcome) uncertainties in the measured phase in the polarization modulation experiment, only the amplitude of the Faraday/Kerr rotation was considered reliable. Unfortunately this is a somewhat insensitive method of probing the cyclotron frequency. As one can see from Fig. 8, the rotation spectrum does not differ much using 0.35m_e or 0.20m_e in the amplitude plot. To fit the data accurately when $\omega_c\tau \sim 1$, one needs to fit the complex Faraday rotation; the peak in imaginary part ($-\theta_K''$) approximately gives the direction evidence for cyclotron resonance. Ref.[1] did not observe obvious signature for CRs because of measuring amplitude of Kerr rotation with poor resolution. In this regard, phase sensitive time-domain THz spectroscopy is a powerful tool to study cyclotron resonances in topological insulators of current generation. Despite the differences in these numbers, the Bi_2Se_3 samples we measured in this paper are similar to those in Ref[1] and the qualitative conclusion that TSSs dominates made in Ref[1] remains.

VII. ASSUMPTION OF NEARLY EQUAL CONTRIBUTION OF THE TOP AND BOTTOM SURFACE STATES

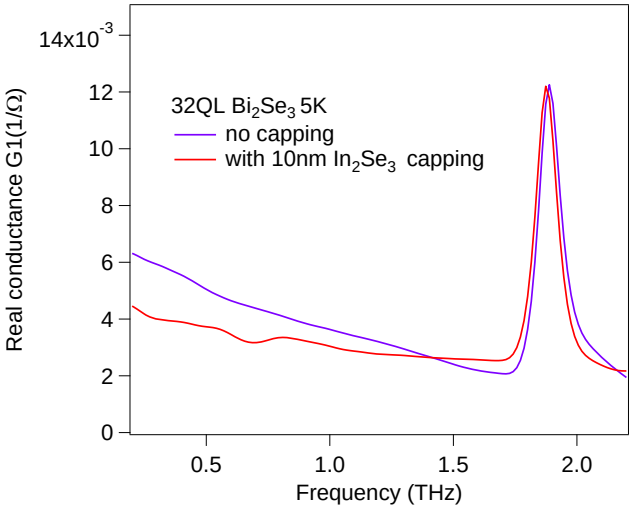

FIG. 9: (Color online) Real conductance of 32 QL Bi_2Se_3 with and without 10nm In_2Se_3 capping at 5 K.

In the main text, we showed that the carrier density estimated by using the spectral weight and mass from the Faraday rotation fits is close to the value obtained using spectral weight from Faraday rotation fit and surface state dispersion. This shows the assumption of nearly equal contributions from the top and bottom surface states is a good approximation. Similarly, DC transport have both shown the chemical potential of the two surface states differed by around 50 meV[19].

A method was discussed in Ref.[20] to distinguish the contribution of the two surfaces from each other. Unfortunately, it appears that the interface between In_2Se_3 and Bi_2Se_3 which present in the In_2Se_3 capped samples used in that work is not as simple as assumed in Ref.[20]. It was been found that there is 20-30% Indium diffusion into the Bi_2Se_3 layer in a recent study[21]. The topological phase transition occurs near x$\sim$ 6 % in $(Bi_{1-x}In_x)_2Se_3$[2,22]. Therefore, the interface of In_2Se_3 and Bi_2Se_3 is not the boundary of normal band insulator and topological insulator. Indium probably diffuses into Bi_2Se_3 layer with a gradient. The true interface TSS must be buried deeply and exist in a background of high disorder. Due to Indium diffusion, the interface which hosts SSs could be $(Bi_{0.06}In_{0.94})_2Se_3$ / $(Bi_{0.045}In_{0.955})_2Se_3$. This hypothesis may explain that the conduction band minimum is positioned only $\sim$ 80 meV above the Dirac point, because the bulk gap decreases when approaching the topological phase transition point at $x \sim 6$ %. Also, more Indium substitution reduces the total carrier density[22], which could be the reason that the top surface has a lower carrier density as discussed in Ref.[20]. We also measured a 32 QL Bi_2Se_3 film capped by 10 nm In_2Se_3. This sample has lower spectral weight and a larger scattering rate, as shown in Fig. 9.

VIII. ROLE OF COPPER

The majority of Cu was found to be Cu^{0+} (neutral) by X-ray photo-emission spectroscopy in this batch of samples[4]. Our data supports this scenario. If 2% Cu substitutes for Bi, then we would observe the shift of phonon frequency as we did in the $(Bi_{1-x}In_x)_2Se_3$ case. In $(Bi_{1-x}In_x)_2Se_3$, we can observe a shift of the phonon at x$\sim$ 1%. Also note that Cu has around half of the atomic number of In, which means 2% Cu substitution would shift the phonon frequency more than In substituted case. Normal Bi_2Se_3 is known to have a conducting bulk with chemical potential 350$\sim$450 meV due to Se vacancies. In keeping with Ref.[4], we believe Cu incorporation passivates Se vacancies, so the carrier density is reduced. We encourage more work to be done to resolve the role of copper by other methods such as STM measurements and first-principle DFT calculations.

IX. BAND BENDING

Topological Insulators can be understood as special narrow-gap semiconductors with surface states. Therefore, band bending effects can be important in such systems. Ref.[4] has a nice summary about band bending in TIs. Here we re-emphasize its importance. The bulk chemical potential for normal Bi_2Se_3 is pinned near the conduction band minimum (therefore $\sim$ 220 meV above Dirac point)[4,23], while the surface state chemical potential is $\sim$ 350 meV in our samples. Downward band bending

results in accumulation layers. From magneto-THz measurements, we concluded that any accumulation layer carriers have a large scattering rate, are essentially featureless in the Faraday rotation and count for less than 10 % of total conductance at low frequencies. For $Cu_{0.02}Bi_2Se_3$, the chemical potential at the surface is ~ 150 meV above the Dirac point, and therefore upwards band bending must occur. ARPES can play an essential role in determining whether a material is a topological insulator by counting if the number of surface state branches is odd or even, but it is not the best tool to conclude whether a TI is bulk-insulating or not due to its extreme surface sensitivity and band bending. For example, upwards band bending was reported in bulk-conducting TIs[23] where ARPES did not observe bulk states but SdH saw a dominating bulk contribution. The most effective way to probe bulk-insulating TIs is through transport measurements. In DC transport, if the carrier density contributing to SdH oscillations is equal to the total carrier density measured by the Hall effect, then the bulk is insulating[4]. In AC optics, if the carrier density contributing to cyclotron resonance is equal to the total carrier density in the Drude term of the zero field conductance, one can conclude that the bulk is insulating.

---

* Electronic address: lwu29@jhu.edu
† Present address: Department of Materials Science and Engineering, Pennsylvania State University, University Park, Pennsylvania 16801, USA.
‡ Electronic address: npa@jhu.edu

[1] R. Valdés Aguilar, A. V. Stier, W. Liu, L. S. Bilbro, D. K. George, N. Bansal, L. Wu, J. Cerne, A. G. Markelz, S. Oh, et al., Phys. Rev. Lett. **108**, 087403 (2012).
[2] L. Wu, M. Brahlek, R. V. Aguilar, A. V. Stier, C. M. Morris, Y. Lubashevsky, L. S. Bilbro, N. Bansal, S. Oh, and N. P. Armitage, Nature Physics **9**, 410 (2013).
[3] N. Bansal, Y. Kim, M. Brahleck, E. Edrey, and S. Oh, Phys. Rev. Lett. **109**, 116804 (2012).
[4] M. Brahlek, N. Koirala, M. Salehi, N. Bansal, and S. Oh, Phys. Rev. Lett. **113**, 026801 (2014).
[5] R. Valdés Aguilar, L. Wu, A. V. Stier, L. S. Bilbro, M. Brahlek, N. Bansal, S. Oh, and N. P. Armitage, J. Appl. Phys. **113**, 153702 (2013).
[6] C. Morris, R. Valdés Aguilar, A. Stier, and N. Armitage, Optics Express **20**, 12303 (2012).
[7] L. Wu, M. Brahlek, R. V. Aguilar, A. V. Stier, C. M. Morris, Y. Lubashevsky, L. S. Bilbro, N. Bansal, S. Oh, and N. P. Armitage, Nature Physics **9**, 410 (2013), supplemetary Information.
[8] Y. Cao, J. Waugh, X. Zhang, J. Luo, Q. Wang, T. Reber, S. Mo, Z. Xu, A. Yang, J. Schneeloch, et al., Nature Physics **9**, 499 (2013).
[9] Y. Zhang, K. He, C. Chang, C. Song, L. Wang, X. Chen, J. Jia, Z. Fang, X. Dai, W. Shan, et al., Nature Physics **6**, 584 (2010).
[10] C. H. Yang, F. M. Peeters, and W. Xu, Phys. Rev. B **82**, 075401 (2010).
[11] W.-K. Tse and A. H. MacDonald, Phys. Rev. Lett. **105**, 057401 (2010).
[12] O. E. Raichev and F. T. Vasko, *Quantum Kinetic Theory and Applications* (Springer, 2005).
[13] D. Culcer and S. Das Sarma, Phys. Rev. B **83**, 245441 (2011); D. Culcer, E. H. Hwang, T. D. Stanescu, and S. Das Sarma, Phys. Rev. B **82**, 155457 (2010).
[14] T. Ando and Y. Uemura, J. Phys. Soc. Jpn. **36** 959, (1974); T. Ando, J. Phys. Soc. Jpn. **36** 1521 (1974); **37** 622 (1974); **37** 1233 (1974).
[15] N. H. Shon and T. Ando, J. Phys. Soc. Jpn **67**, 2421 (1998); Y. Zheng and T. Ando, Phys. Rev. B**65**, 245420 (2002).
[16] I. Dmitriev, A. Mirlin, D. Polyakov, and M. Zudov, Reviews of Modern Physics **84**, 1709 (2012).
[17] C.-X. Liu, X.-L. Qi, H. Zhang, X. Dai, Z. Fang, and S.-C. Zhang, Phys. Rev. B **82**, 045122 (2010).
[18] G. Refael, Private Communication.
[19] Y. Xu, I. Miotkowski, C. Liu, J. Tian, H. Nam, N. Alidoust, J. Hu, C.-K. Shih, M. Z. Hasan, and Y. P. Chen, Nature Physics **10**, 956 (2014).
[20] G. S. Jenkins, D. C. Schmadel, A. B. Sushkov, H. D. Drew, M. Bichler, G. Koblmueller, M. Brahlek, N. Bansal, and S. Oh, Phys. Rev. B **87**, 155126 (2013).
[21] H. Lee, C. Xu, S. Shubeita, M. Brahlek, N. Koirala, S. Oh, and T. Gustafsson, Thin Solid Films **556**, 322 (2014).
[22] M. Brahlek, N. Bansal, N. Koirala, S.-Y. Xu, M. Neupane, C. Liu, M. Z. Hasan, and S. Oh, Phys. Rev. Lett. **109**, 186403 (2012).
[23] J. G. Analytis, J.-H. Chu, Y. Chen, F. Corredor, R. D. McDonald, Z. X. Shen, and I. R. Fisher, Phys. Rev. B **81**, 205407 (2010).